**Title**

In Vivo Expression of a Light-Activatable Potassium Channel Using Unnatural Amino Acids

**Authors**

Kang, Ji-Yong
Kawaguchi, Daichi
Coin, Irene
et al.

Peer reviewed

# In vivo Expression of a Light-activatable Potassium Channel Using Unnatural Amino Acids

**Ji-Yong Kang**[1], **Daichi Kawaguchi**[2], **Irene Coin**[1], **Zheng Xiang**[1], **Dennis D. M. O'Leary**[2], **Paul A. Slesinger**[3,4], and **Lei Wang**[1,*]

[1]Chemical Biology and Proteomics Laboratory, The Salk Institute for Biological Studies, La Jolla, CA 92037, USA

[2]Molecular Neurobiology Laboratory, The Salk Institute for Biological Studies, La Jolla, CA 92037, USA

[3]Peptide Biology Laboratory, The Salk Institute for Biological Studies, La Jolla, CA 92037, USA

[4]Department of Neuroscience, Icahn School of Medicine at Mount Sinai, New York, NY 10029, USA

## SUMMARY

Optical control of protein function provides excellent spatial-temporal resolution for studying proteins *in situ*. Although light-sensitive exogenous proteins and ligands have been employed to manipulate neuronal activity, a method for optical control of neuronal proteins using unnatural amino acids (Uaa) *in vivo* is lacking. Here, we describe the genetic incorporation of a photoreactive Uaa into the pore of an inwardly-rectifying potassium channel Kir2.1. The Uaa occluded the pore, rendering the channel non-conducting, and upon brief light illumination, was released to permit outward $K^+$ current. Expression of this photo-inducible inwardly rectifying potassium (PIRK) channel in rat hippocampal neurons created a light-activatable PIRK switch for suppressing neuronal firing. We also expressed PIRK channels in embryonic mouse neocortex *in vivo* and demonstrated a light-activated PIRK current in cortical neurons. The principles applied here to a potassium channel could be generally expanded to other proteins expressed in the brain to enable optical regulation.

## INTRODUCTION

The ability to control protein function with light provides excellent temporal and spatial resolution for precise investigation *in vitro* and *in vivo*, and thus is having significant impact on neuroscience. For example, naturally light-sensitive opsin channels and pumps have been exploited to excite or inhibit neurons, enabling specific modulation of selected cells and circuits in diverse model organisms (Bernstein and Boyden, 2011; Fenno et al., 2011; Yizhar et al., 2011). However, since this approach relies on the ectopic expression of an exogenous or chimera protein requiring retinal as the chromophore, it cannot be applied to control a

*Correspondence: lwang@salk.edu.

**SUPPLEMENTAL INFORMATION**
Supplemental Information includes 5 figures, 1 supplemental text, and supplemental experimental procedures.

particular endogenous protein. Another elegant method engineers light responsiveness into endogenous receptors and channels by chemically tethering a photo-switchable azobenzene-coupled ligand (Szobota and Isacoff, 2010). The ligand is presented or withdrawn from the binding site of the protein through the photo-isomerization of the azobenzene moiety. This approach cannot address proteins that are expressed but failed to conjugate with the azobenzene-coupled ligand, and ligand tethering has been limited to the extracellular side of membrane proteins, excluding the intracellular side and intracellular proteins.

Photo-responsive unnatural amino acids (Uaas) provide another flexible avenue for optical control of proteins activities. Microinjection of tRNAs chemically acylated with Uaas allows the incorporation of photocaging groups into receptors and ion channels in *Xenopus oocytes*, which have revealed novel insights on their structure and function (England et al., 1997; Miller et al., 1998; Philipson et al., 2001). The requirement of microinjection has mainly limited this approach to large oocytes. Genetically encoding Uaas with orthogonal tRNA/synthetase pairs enables the Uaa to be incorporated into proteins with high protein yields in mammalian cells and organisms (Liu and Schultz, 2010; Wang et al., 2001; Wang et al., 2006; Wang et al., 2009), providing potential for studying proteins with Uaas directly in primary neurons and mouse models (Shen et al., 2011; Wang et al., 2007). A challenge in the neuroscience field, however, has been the application of Uaa technology in mammalian neurons *in vitro* and ultimately in the mouse brain *in vivo*.

Here we demonstrate the optical control of a neuronal protein *in vitro* and *in vivo* using a genetically encoded photoreactive Uaa. Kir2.1 is a strong inwardly-rectifying potassium channel that is crucial in regulating neuronal excitability, action potential cessation, hormone secretion, heart rate, and salt balance (Bichet et al., 2003). We incorporated 4,5-dimethoxy-2-nitrobenzyl-Cysteine (Cmn) into the pore of Kir2.1, generating a photo-activatable inwardly rectifying potassium (which we refer to as 'PIRK') channel. Light activation of PIRK channels expressed in rat hippocampal neurons suppressed neuronal firing. In addition, we expressed PIRK channels in embryonic mouse neocortex and measured light-activated PIRK current in cortical neurons, and showed the potential for its use in other brain regions such as diencephalon, demonstrating for the first time the successful implementation of the Uaa technology *in vivo* in the mammalian brain. Genetically encoding Uaas has no limitations on protein type and location (Wang and Schultz, 2005), and photocaging is compatible with modulating various proteins (Adams and Tsien, 1993; Fehrentz et al., 2011). We therefore expect our method can be generally applied to other brain proteins, enabling optical investigation of a range of channels, receptors, and signaling proteins in the brain.

## RESULTS

### Construction of a PIRK Channel with Genetically Encoded Photocaged Uaa

Potassium ions flow through the central pore of Kir2.1 channels (Ishii et al., 1994; Kubo et al., 1993). We reasoned that incorporation of an Uaa with a bulky side chain might occlude the channel pore and restrict current flow. Photolysis of the Uaa would enable release of the bulky side chain moiety and restore current flow through the channel, thus creating a photo-activatable inwardly rectifying potassium channel, PIRK (Figure 1A). Ideally, a natural amino acid residue can be regenerated from the Uaa after photolysis, minimizing potential perturbation to protein structure and function. 4,5-Dimethoxy-2-nitrobenzyl-Cysteine (Cmn) is a perfect Uaa for constructing a PIRK channel. The dimethoxynitrobenzyl group of Cmn is readily hydrolyzed by UV light, releasing the cage group and becoming Cys (Figure 1B, Figure S2A) (Rhee et al., 2008). Compared to the conventional photocaging *o*-nitrobenzyl group, the dimethoxynitrobenzyl group is bulkier and has a higher quantum yield to facilitate photolysis. Previously, 4,5-dimethoxy-2-nitrobenzyl serine was incorporated into

the transcription factor Pho4 in *Saccharomyces cerevisiae* to control phosphorylation with light (Lemke et al., 2007). Based on the similar structure and characteristics between serine and cysteine, we hypothesized that the orthogonal $tRNA_{CUA}^{Leu}$/synthetase pair evolved in yeast to incorporate 4,5-dimethoxy-2-nitrobenzyl serine might also selectively incorporate Cmn. Indeed, Cmn was efficiently incorporated into proteins in mammalian cells by this pair, which we refer to as $tRNA_{CUA}^{Leu}$/CmnRS for clarity. Cmn was chosen for incorporation because multiple sites of Kir2.1 are found permissive for Cys mutation and the sulfhydryl group of Cys also provides a chemically reactive functionality for possible secondary modifications if required.

To achieve photo-activation of Kir2.1 using Cmn, we considered the following criteria for identifying a target site for incorporation into the channel protein: (1) the site should reside in the channel pore where the side chain of Cmn would face the pore lumen and be easily removed following photocleavage; (2) the pore should be large enough to accommodate four Cmn molecules in a Kir2.1 tetramer without disrupting protein folding, but small enough to efficiently inhibit ion current flow; and (3) a site where a Cys mutation would not likely interfere with Kir2.1 function.

Using published data on Kir2.1 pore topology and function (Kubo et al., 1993; Lu et al., 1999a; Minor et al., 1999; Tao et al., 2009) and the crystal structure of chicken Kir2.2 (Tao et al., 2009), we identified fifteen amino acids in the pore of rat Kir2.1 (which has 76% sequence homology with chicken Kir2.2) with side chains that face the pore lumen (K117, V118, A131, T142, I143, C149, V150, D152, S165, C169, D172, I176, M180, A184, and E224). Previous studies indicated that Cys substitution at T142, I143, D172, I176, A184, or E224 did not interfere with Kir2.1 function (Dart et al., 1998; Kubo et al., 1998; Lu et al., 1999a; Lu et al., 1999b; Minor et al., 1999; Xiao et al., 2003). Therefore, these six amino acids plus C149 and C169 were selected for Cmn incorporation (Figure 2A, Figure S1A–B).

The codon for these candidate sites was first mutated to the amber stop codon TAG to generate eight different mutant Kir2.1 (Kir2.1$_{TAG}$) genes. The Kir2.1$_{TAG}$ cDNA was individually coexpressed with the orthogonal $tRNA_{CUA}^{Leu}$/CmnRS pair in human embryonic kidney 293T (HEK293T) cells. Upon exogenous addition of the Uaa Cmn to growth media, the CmnRS aminoacylates Cmn onto the $tRNA_{CUA}^{Leu}$, which in turn recognizes the amber stop codon (UAG) in Kir2.1 mRNA and incorporates Cmn into Kir2.1 protein during translation (Wang et al., 2001; Wang and Schultz, 2005).

Each candidate site was initially tested whether it was permissive for UAG suppression by the orthogonal $tRNA_{CUA}^{Leu}$/leucyl−tRNA synthetase (LeuRS) pair, which incorporates the natural amino acid leucine (Leu). Each Kir2.1$_{TAG}$ gene was transfected into HEK293T cells along with the $tRNA_{CUA}^{Leu}$/LueRS (Figure 2B). The gene for green fluorescent protein (GFP) engineered with an amber stop codon at Tyr182 (GFP_Y182$_{TAG}$) was co-transfected (Wang et al., 2007). GFP fluorescence would indicate the successful suppression of the UAG stop codon by the orthogonal tRNA/synthetase. The function of individual Kir2.1$_{TAG}$ channels was then determined by whole-cell patch-clamp recordings from GFP-positive cells. For example, a green-positive HEK293T cell transfected with Kir2.1_C169$_{TAG}$ and the $tRNA_{CUA}^{Leu}$/LueRS produced a basally active inwardly rectifying current that was inhibited by extracellular $Ba^{2+}$ ($I_{Kir}$), similar to wild-type Kir2.1 channels (Figure 2C). Of the eight candidate sites, $I_{Kir}$ currents measured at −100 mV from HEK293T cells expressing Kir2.1_I143$_{TAG}$, Kir2.1_C149$_{TAG}$, Kir2.1_C169$_{TAG}$, or Kir2.1_I176$_{TAG}$ were significantly larger than those from untransfected cells (Figure 2D), indicating successful suppression and incorporation of Leu.

If a functional Kir2.1 channel could be generated through Leu incorporation at the TAG site, then it seemed likely the same site would be compatible for the larger Uaa Cmn. We therefore tested Kir2.1_I143$_{TAG}$, Kir2.1_C149$_{TAG}$, Kir2.1_C169$_{TAG}$, and Kir2.1_I176$_{TAG}$ for functional incorporation of Cmn (Figure 2E–H, Figure S1C). HEK293T cells were transfected with cDNAs for the Kir2.1$_{TAG}$ channel, $\text{tRNA}^{\text{Leu}}_{\text{CUA}}$/CmnRS and the GFP_Y182$_{TAG}$ reporter (Figure 2B), and incubated in Cmn (1 mM) for 12–24 hrs. Functional incorporation of Cmn was expected to either lead to a basally active $I_{Kir}$ or to $I_{Kir}$ that is revealed upon brief (1 sec) light illumination (385 nm at 40 mW/cm$^2$). For HEK293T cells expressing Kir2.1_I143$_{TAG}$ or Kir2.1_I176$_{TAG}$, we could detect no $I_{Kir}$ before or after light illumination, indicating either no amber suppression or a non-functional channel after Cmn incorporation (Figure 2E, Figure S1C). By contrast, HEK293T cells expressing Kir2.1_C149$_{TAG}$ displayed a large $I_{Kir}$ that was unchanged by light illumination (Figure 2F), suggesting incorporation of Cmn at C149 did not significantly occlude the pore. Strikingly, HEK293T cells expressing Kir2.1_C169$_{TAG}$ displayed little $I_{Kir}$ at negative membrane potentials that increased significantly upon light illumination (Figure 2G–H). These results suggested that incorporation of Cmn at C169 largely occludes the channel pore and that the blocking particle is released following brief light stimulation, indicating the successful construction of a photo-activatable Kir2.1 channel.

## Light-dependent Activation of PIRK in HEK293T Cells

We next examined the light-sensitivity features of Kir2.1_C169$_{TAG}$Cmn (referred to as PIRK) channels expressed in HEK293T cells. To enhance channel expression, we fused the fluorescent protein mCitrine (mCit) to the C-terminus of Kir2.1_C169$_{TAG}$ (Figure 3A), which reduced the number of plasmids needed for transfection and allowed tracking the location of PIRK channels. Fusion of GFP to the C-terminus of Kir2.1 was shown previously to not affect Kir2.1 channel physiology (Sekar et al., 2007). Addition of Cmn to the bath resulted in fluorescently labeled HEK293T cells (Figure 3B, Figure S2A) and the expression of full-length Kir2.1-GFP fusion protein (Figure S2B). A brief (1 sec) pulse of UV light (385 nm LED, 40 mW/cm$^2$) led to activation of an inwardly rectifying current that was blocked by Ba$^{2+}$ (Figure 3C,D). The activation kinetics had fast and slow components with time constants ( ) of 298 ± 134 ms and 15.0 ± 4.3 sec, respectively (n = 7). Note the amplitude of light-activated current is larger than that in Figure 2H, indicating that PIRK expression level increased with the two plasmid system. When incorporated with Leu, Kir2.1_C169$_{TAG}$Leu channels showed large $I_{Kir}$ (8.30 ± 1.48 nA, n = 7), which was not affected by light illumination (data not shown). On the other hand, HEK293T cells expressing PIRK (Kir2.1_C169$_{TAG}$Cmn) channels produced no or negligible $I_{Kir}$ before UV light (0.14 ± 0.07 nA, n = 10 vs. 0.05 ± 0.02 nA, n = 9 for untransfected; *P* > 0.05, unpaired t-test), and marked increase in $I_{Kir}$ after UV light (1.65 ± 0.41 nA, n = 10) (Figure 3E). The smaller $I_{Kir}$ for PIRK compared to Kir2.1_C169$_{TAG}$Leu was likely due to the less efficient aminoacylation with CmnRS and therefore less Cmn incorporation.

To investigate the relationship between the light dosage and current activation, we varied the duration and frequency of UV light pulses. Single light pulses with different lengths were applied to cells expressing PIRK channels. Using a 40 mW/cm$^2$ LED light source, one second and 500 ms light pulses evoked similar amount of current at −100 mV (2.27 ± 0.51 nA, n = 5 for 1 sec; 2.04 ± 0.39 nA, n = 5 for 500 ms). Shorter UV pulses (200 ms, 100 ms, and 50 ms) led to progressively smaller currents (Figure 3F). No significant change in current amplitude was measured with a single 20 ms light pulse (n = 6, data not shown). We next investigated the effect of sequential UV light pulses. Sequentially delivered light pulses of 200 ms duration each led to stepwise activation of PIRK channels (Figure 3G). Fewer UV pulses were required to maximally activate PIRK channels with longer duration UV light

pulses (Figure 3H). Together, these results illustrate that modulating the duration and number of light pulses can be used to fine-tune the extent of PIRK current activation.

## Light-activation of PIRK Suppresses Neuronal Firing

A significant obstacle in using Uaa technology has been the implementation of Uaa in vertebrate neurons. We therefore investigated the expression of PIRK channels in primary cultures of hippocampal neurons. Transfection of rat hippocampal primary neurons with the cDNA for PIRK-mCit and $tRNA_{CUA}^{Leu}/CmnRS$ (Figure 3A) led to fluorescence in cultures exposed to Cmn for 12–48 hrs (Figure 4A), indicating the successful incorporation of Cmn into PIRK channels. The expression of PIRK in neurons appeared similar to the pattern of endogenous Kir2.1 channels (Figure S3). Moreover, PIRK expression did not appear to change the basic membrane properties of the neurons (Figure S4A–C). Whole-cell patch-clamp recordings from mCitrine positive neurons revealed no significant increase in basal inward current at negative potentials ($-0.21 \pm 0.06$ nA, n = 6 vs $-0.43 \pm 0.09$ nA, n = 6; $P > 0.05$, unpaired t-test). However, UV light stimulation (1 sec, 40 mW/cm$^2$) induced a large inwardly rectifying current in PIRK (+Cmn) cells (Figure 4B). By contrast, control neurons without PIRK showed little or no response to UV light (Figure 4B, 4C, Figure S4D). In PIRK-expressing neurons incubated with Cmn, UV light induced a mean inward current of $-0.46 \pm 0.18$ nA (at $-100$ mV), consistent with unblock of constitutively open Kir2.1 channels (Figure 4C, Supplemental Text S1).

We next examined the effect of PIRK activation on the excitability of hippocampal neurons. Activation of an inwardly rectifying K$^+$ current would be expected to significantly reduce neuronal excitability by the outward flow of K$^+$ current through Kir channels (Burrone et al., 2002; Yu et al., 2004). In whole-cell current-clamp recordings, a range of current injections (range: 10–190 pA, mean $\pm$ s.e.m.: $45 \pm 4$ pA, n = 56) were used to induce continuous firing of action potentials (5–15 Hz) in both control neurons and PIRK-expressing neurons (Figure 4D,E). The induced membrane potential was relatively consistent from cell to cell (Figure 4G). In PIRK-expressing neurons, action potential firing stopped abruptly upon brief UV light stimulation (1 sec, 40 mW/cm$^2$). Importantly, addition of Ba$^{2+}$ to the bath restored action potential firing (Figure 4D), confirming that the observed suppression of activity was due to activation of Kir2.1 channels. Neither light illumination nor Ba$^{2+}$ addition altered the excitability of control neurons (Figure 4E, Figure S4E–F). In multiple recordings from different preparations of hippocampal neuronal cultures, we consistently observed a significant decrease in firing frequency in PIRK-expressing neurons (+Cmn) following UV light, which was restored to normal levels of firing in the presence of extracellular Ba$^{2+}$ (Figure 4F). In control neurons, we observed no significant change in firing frequency after light activation or Ba$^{2+}$ addition (Figure 4F).

Plotting the membrane potential induced by the current step before and after UV light stimulation showed a clear hyperpolarization in PIRK-expressing (+Cmn) neurons following UV light (Figure 4G, Figure S4H). Furthermore, subsequent extracellular Ba$^{2+}$ reproducibly depolarized the membrane potential. Taken together, these experiments demonstrate that UV light activation of PIRK channels provides a technique for spatially inhibiting neuronal activity through membrane hyperpolarization.

To explore the dynamic range of PIRK's effect on neuronal firing, we measured the firing frequency from each neuron over a range of current injections (0–70 pA). Cells that did not fire throughout the current range were excluded. With small current injections (< 40 pA), the firing frequency decreased significantly upon UV light activation of PIRK channels (Figure 5A). With larger current injections (40–70 pA) and higher firing frequencies, however, there was no significant change in firing frequency following UV light illumination of PIRK-

expressing neurons. This ceiling effect can be explained by the native properties of strong inwardly rectifying Kir2.1 channels, which conduct little outward current at positive membrane potentials (Ishii et al., 1994; Kubo et al., 1993). Kir channels are well known for their ability to hyperpolarize membranes and increase the threshold for firing an action potential. To examine this, we measured the minimum amount of current required to evoke an action potential (referred to as rheobase). The rheobase increased in PIRK-expressing neurons following UV light exposure (Figure 5C). UV light activation of PIRK also hyperpolarized the resting membrane potential of PIRK-expressing neurons by −17 mV, whereas UV light had no effect on the resting potential of control neurons (Figure 5D, Figure S4G).

## In vivo Expression of PIRK in the Mouse Neocortex

Having successfully expressed PIRK channels in dissociated hippocampal neurons, we next attempted to express PIRK channels *in vivo*. Genetically encoding Uaas using orthogonal tRNA/synthetase has great potential to address challenging biological questions *in vivo*, but this technology has yet to be applied in mammals. There were two main challenges for *in vivo* incorporation of Uaas in mammals: (1) efficient delivery and expression of the genes for the orthogonal tRNA/synthetase and the target protein into specific tissue or cells; and (2) sufficient bioavailability of the Uaa at the target tissue and cells. We chose mouse embryos for genetically incorporating Uaas into the brain because of the ability to introduce cDNA and chemicals *in utero*, and then to prepare brain slice pre- and post-natally (Mulder et al., 2008; Saito, 2006; Tabata and Nakajima, 2001).

We started addressing the first challenge by attempting to incorporate Leu, an endogenously available amino acid, into GFP through UAG suppression in mouse embryonic brain. The $GFP\_Y182_{TAG}$ reporter gene was encoded on the same plasmid with the orthogonal $tRNA_{CUA}^{Leu}$ (Figure 6A). Three copies of this tRNA expression cassette driven by the H1 promoter were included to increase the UAG suppression efficiency, as we previously demonstrated in mammalian cells (Coin et al., 2011). A red fluorescent protein mCherry was coexpressed with the orthogonal LeuRS through IRES on the other plasmid to indicate successful gene delivery *in vivo*. Genes were introduced in the mouse neocortex using *in utero* electroporation, and four days later the embryonic cortical sections were prepared and fluorescently imaged to check gene expression (Figure 6C). Electroporation of the LeuRS-IRES-mCherry plasmid alone showed red fluorescence, indicating mCherry served as a good indicator for gene delivery (Figure 6D, top row). Co-delivery of the $tRNA_{CUA}^{Leu} - GFP_{TAG}$ plasmid with a separate plasmid encoding mCherry showed mCherry fluorescence but no GFP fluorescence, demonstrating that there was no background read-through of the UAG stop codon in the GFP mRNA (Figure 6D, middle row). On the other hand, GFP fluorescence was now observed in the neocortices of mice electroporated with $tRNA_{CUA}^{Leu}$, $GFP_{TAG}$, and LeuRS cDNA (Figure 6D, bottom row). In addition, all green fluorescent cells had red fluorescence, indicating that translation of full-length GFP required both the $tRNA_{CUA}^{Leu}$ and the LeuRS to suppress the UAG codon. Therefore, these results suggest the successful *in vivo* incorporation of Leu into GFP through UAG suppression.

Incorporation of an Uaa *in vivo* presented an additional challenge. For the convenience of detection, we initially tried to incorporate Cmn into $GFP_{TAG}$ in the mouse brain using a unique heterochronic approach. The $tRNA_{CUA}^{Leu}$, CmnRS, and $GFP_{TAG}$ genes (Figure 6A) were first electroporated *in utero*, and then after two days, we injected Uaa Cmn directly into the lateral ventricle of the mouse brain (Figure 6C). Without injecting Cmn, no green fluorescence was detected in the neocortical plates (Figure 6E, top row). After injecting Cmn, weak green fluorescence could be detected (not shown). Previously we discovered that

preparation of Uaa in the dipeptide form increases the efficiency of Uaa incorporation in *C. elegans*, possibly because the dipeptide is transported into cells more efficiently than the single Uaa via oligopeptide transporter PEPT1 and PEPT2 (Parrish et al., 2012). Intracellular dipeptide would then be hydrolyzed by cellular peptidases to generate the free Uaa for incorporation. Since PEPT2 is highly expressed in rodent brain (Lu and Klaassen, 2006), Cmn-Ala was adopted to improve Cmn bioavailability. We thus synthesized the Cmn-Ala dipeptide and injected it in the lateral ventricle of the mouse brain. Indeed, with this adjustment we could observe a dramatic improvement, with strong green fluorescence in the neocortex (Figure 6E, bottom row), indicating the successful incorporation of Cmn into $GFP_{TAG}$ *in vivo*.

After overcoming both challenges we proceeded to incorporate Cmn into $Kir2.1\_C169_{TAG}$ to express PIRK channels directly in the mouse brain. The $Kir2.1\_C169_{TAG}$ gene was encoded with the $tRNA_{CUA}^{Leu}$ in one plasmid, and another plasmid encoded the CmnRS together with mCherry as a reporter for gene delivery (Figure 6B). A third plasmid encoding $GFP\_Y182_{TAG}$ was also co-electroporated *in utero*. Detection of GFP fluorescence would indicate the successful delivery of all three plasmids, since UAG suppression in GFP would require both the $tRNA_{CUA}^{Leu}$ and the CmnRS; Cmn incorporation in $GFP_{TAG}$ would suggest Cmn incorporation in $Kir2.1_{TAG}$ as well, because both genes were present in the same cell. As expected, only when all three gene constructs were present and Cmn-Ala was introduced to the brain, green fluorescent cells were observed in the mouse neocortex (Figure 6F). Cells with both red and green fluorescence should have Cmn incorporated into $Kir2.1_{TAG}$ to make PIRK channels.

To verify if functional PIRK channels were expressed in these neurons, whole-cell recordings were conducted on acute slices prepared from the mouse neocortical plates. Indeed, the green and red fluorescent neurons had no inward current at negative holding potential, but a brief pulse of light rapidly activated the inward current (Figure 6G). The current was completely blocked by adding $Ba^{2+}$, confirming it was generated by PIRK. In contrast, control neurons did not show any photo-activated inward current (Figure S5C,D). $I_{kir}$ measured from these PIRK-expressing neurons in the mice neocortical slices was significantly increased upon light activation (Figure 6H). The light-dependent activation of PIRK channels further confirmed the successful incorporation of Cmn into $Kir2.1_{TAG}$ in the mouse brain. In short, these data demonstrate the successful expression of a functional PIRK *in vivo*.

To demonstrate the general utility of this technique for other brain regions, we also performed *in utero* electroporation and *in utero* injection of unnatural amino acids in embryonic diencephalon that included thalamus and hypothalamus. The procedure was similar to that described above for the neocortex, but involved a unique heterochronic procedure with an injection of the $tRNA_{CUA}^{Leu}-GFP_{TAG}$ plasmid and CmnRS-IRES-mCherry plasmid (Figure 6A) into the 3rd ventricle at E13.5 accompanied by electroporation, then later at E16.5 an injection of Cmn-Ala into or near to the 3rd ventricle. The embryos were harvested at E17.5 and the brains analyzed using imaging methods. GFP expression is clearly evident indicating Uaa incorporation into $GFP_{TAG}$ (Figure S5E,F).

## DISCUSSION

Genetically encoding Uaas with orthogonal tRNA/synthetase was initially developed in *E. coli* and later extended to various single cells and recently to invertebrates such as *Caenorhabditis elegans* (Liu and Schultz, 2010; Parrish et al., 2012; Wang et al., 2001; Wang et al., 2009). For neuroscience research, Uaa incorporation in primary neurons (Wang

et al., 2007), neural stem cells (Shen et al., 2011), and animals would permit the use of Uaas to directly address neurobiological processes in the native environment. Previously, Uaas have been incorporated into ion channels and receptors expressed in *Xenopus oocytes* (Beene Darren et al., 2003) and mammalian cells *in vitro* (Wang et al., 2007). Although sufficient for probing the structure and function of a single target protein, heterologous expression systems are not suitable for investigating neuronal signaling and circuits involving a cascade of neuronal proteins or multiple cells. In this report, we describe the methodology for manipulating a neuronal protein directly in primary neurons using genetically encoded Uaas. Moreover, we report the successful incorporation of Uaas into the brain of mouse embryos, which represents to the best of our knowledge the first report on Uaa incorporation in mammals. To overcome the obstacles for Uaa incorporation *in vivo*, we delivered the genes for the orthogonal tRNA/synthetase into mouse neocortex and diencephalon by *in utero* electroporation, and supplied the Uaa to the brain in the form of a dipeptide through injection to the ventricles. The ability to genetically incorporate Uaas into neuronal proteins in mammalian brains provides a novel toolbox for innovative neuroscience research.

The development of optically controlled channels and pumps is a powerful method for analyzing the function of specific neurons in neural circuits (Yizhar et al., 2011). However, the photoresponsiveness of opsin, which depends on the retinal chromophore and its modulation protein domain, cannot be simply transplanted into other proteins without dramatically altering the target protein. Therefore, this approach is not suitable for optical control of proteins natively expressed in neurons. Alternatively, natively expressed channels and receptors can be modified to be controlled by an optically switched ligand. For example, a photoisomerizable azobenzene-coupled ligand can be chemically attached to the glutamate receptor sGluR0 or the potassium channel TREK1 for light gating (Janovjak et al., 2010; Sandoz et al., 2012). A limitation with this technique, however, is that application of the chemical photoswitch has been described for labeling extracellular regions of the target protein, suggesting intracellular proteins may be less amenable to this labeling method. In contrast, genetically encoding photo-reactive Uaas should provide a general methodology for manipulating neuronal proteins, both cytoplasmic and membrane proteins, with light in neurons. Since genetic incorporation of Uaas using orthogonal tRNA/synthetase pairs imposes no restrictions on target protein type, cellular location or the site for Uaa incorporation (Wang and Schultz, 2005), with methods reported herein we expect that various proteins expressed in neurons can be generally engineered with photo-reactive Uaas at an appropriate site to enable optical control. Moreover, a family of photo-reactive Uaas exist (Beene Darren et al., 2003; Liu and Schultz, 2010) that can be fine-tuned for a particular active site in the protein. This flexibility should significantly expand the scope of proteins and neuronal processes subject to light regulation.

Photoactivation of PIRK channels expressed in hippocampal neurons led to constitutive activation of Kir2 channels that produced a sustained suppression of neuronal firing. There are unique features of PIRK that may complement existing methods for neuronal silencing. Archaeorhodopsin-3 (Arch) and halorhodopsin (NpHR) originated from halobacteria are members of the opsin family employed to silence neuronal activity (Chow et al., 2010; Zhang et al., 2007). Illumination of Arch, a proton pump, for extended period of time could result in intra- and extracellular pH disturbance, which could negatively impact on cell health (Han, 2012; Okazaki et al., 2012). Activation of the chloride pump NpHR leads to accumulation of intracellular chloride ions and can compromise $GABA_A$-receptor-mediated inhibition (Raimondo et al., 2012). In addition, continuous activation of Arch or NpHR is limited by its inactivation and potential photo damage, which is not ideal for studies such as epilepsy where it is important to maintain membrane hyperpolarization for a long period of time (Kokaia et al., 2013). In contrast, PIRK is based on Kir2.1, an inward rectifying

potassium channel whose native function is to regulate neuronal excitability (Bichet et al., 2003; Hibino et al., 2010; Nichols and Lopatin, 1997). Through a small amount of outward $K^+$ current, Kir2.1 can directly silence the electrical activity of neurons. In fact, ectopic expression of Kir channels has been used previously over the last decade to investigate the effect of neuronal excitability on circuit function (Burrone et al., 2002; Johns et al., 1999; Nadeau et al., 2000; Yu et al., 2004). By endowing Kir2.1 with photo-responsiveness in PIRK, we have provided the ability to temporally control through light precision the activation of Kir2 channels. Another advantage of PIRK is that it functions like a binary switch, whereby a single light pulse can induce the lasting silencing effect on target neurons. Without the need to continuously deliver light through the optical fiber, this binary switch feature of PIRK is convenient for animal studies to mitigate potential interference of light or light devices on animal behavior, and could therefore be useful for studying or treating intractable epilepsy, intractable pain, or muscle spasms. Moreover, PIRK channels may be utilized for studying a variety of physiological processes and diseases that directly involve Kir2.1 channels. For example, Kir2.1 function has been implicated Andersen syndrome (Plaster et al., 2001), cardiac short Q-T syndrome (Priori et al., 2005), and osteoblastogenesis (Zaddam et al., 2012).

PIRK is designed with a photo-releasable pore-blocking group. This "block-and-release" strategy may be generally applicable to other channels and receptors. For instance, G protein-gated Kir channels (Kir3 family), -amino-3-hydroxy-5-methyl-4-isoxazolepropionic acid receptors (AMPARs), and *N*-Methyl-D-aspartic acid receptors (NMDARs) share similar pore topology with Kir2.1. By incorporating Cmn into pore residues in these proteins, one should be able to similarly install light-responsiveness to them for highly disciplined study of channel/receptor physiology. On a broader perspective, it is also possible to expand the Uaa-based optical control to the function of other proteins beyond ion channels and receptors. Multiple amino acids such as tyrosine, serine, lysine, glutamate, aspartate, and glycine have been caged with different photo-releasable groups (Beene Darren et al., 2003), and some of them can be genetically encoded in *E. coli*, yeast, and mammalian cells (Liu and Schultz, 2010; Wang et al., 2009). Using methods described in this report, these amino acids can be similarly photocaged for optical control of various protein functions in neurons. For instance, by photocaging appropriate amino acids it should be possible to block-and-release protein-protein interaction, protein-nucleic acid interaction, access of an active site, or access of posttranslational modification sites in neurons. In addition, *in vivo* Uaa incorporation, as demonstrated in the embryonic mouse neocortex and diencephalon here, has the potential to be extended to other regions of the brain, adult animals and more mammals. Genetic knockin or viral delivery (Shen et al., 2011) can be used to express the orthogonal tRNA/synthetase and target protein in transgenic and adult animals, respectively. Some Uaas may be bioavailable through food or water feeding; others can be prepared in the dipeptide format shown here and injected directly into the brain ventricles. Moreover, optical control via Uaa can be made compatible with two-photon activation. Protecting groups efficient for two-photon photolysis have been developed for caging amino acids (Matsuzaki et al., 2001). In the future it may be possible to genetically incorporate azobenzene-containing Uaas into neurons for reversible optical control (Bose et al., 2006). In summary, the new methodology presented here serves as a solid basis for optically controlling a variety of neuronal proteins in studies of neurobiological processes in the brain.

## EXPERIMENTAL PROCEDURES

### Electrophysiology and Light Activation in Culture

Whole-cell patch clamp was used to record macroscopic currents with an Axopatch 200B (Molecular Devices, Axon Instruments) amplifier. Currents were adjusted electronically for

cell capacitance and series resistance (80–100%), filtered at 1 kHz with an 8-pole Bessel filter and digitized at 5 kHz with a Digidata 1200 interface (Molecular Devices). For voltage-clamp recordings, currents were elicited with voltage ramp from −100 mV to +50 mV delivered at 0.5 Hz. For some recordings, cells were held at −100 mV continuously. For current-clamp recordings, the resting potential was first adjusted to around −72 mV by injecting small current. Afterwards, a step current was injected to induce 5–15 Hz continuous firing of action potentials. For Cmn photolysis, an LED with emission of 385 nm (~40 mW; Prizmatix, Israel) was externally installed at the microscope to deliver light to the cell from 1 cm away at 45° angle. Light power at the sample was measured 40 mW/cm$^2$. Light pulse was signaled from the amplifier through the digitizer. Data are expressed as mean ± s.e.m. and statistical significance ($P < 0.05$) were determined by one-way analysis of variance (ANOVA) with Newman-Keuls test or Student's t test. All measurements were made at room temperature.

### *In utero* Electroporation and *in utero* Injection of Unnatural Amino Acids

Introduction of plasmid DNA into the neuroepithelial cells of mouse embryonic neocortex *in utero* was performed as described (Tabata and Nakajima, 2001) with minor modifications. In brief, the uterine horns were exposed at embryonic day 14.5 (E14.5), and ~1 μl DNA solution (0.2–5 μg/μl of each plasmid, depending on the construct) was injected into the lateral ventricle of each littermate. Embryos were then electroporated with an electroporator CUY21EDIT (BEX, 0.5 cm puddle type electrode, 33–35 V, 50 ms duration, 4–8 pulses). After electroporation, the uterine horns were returned to the abdominal cavity to allow the embryos to continue development. For Leu incorporation (Figure 6D), the embryos were harvested four days after electroporation, and the brains were then subjected to the imaging analysis. For Cmn incorporation (Figure 6E–H), the uterine horns were exposed again at E16.5, and Cmn (500 mM, 2–5 μl) was injected to the electroporated side or both sides of the lateral ventricle. The uterine horns were placed back into the abdominal cavity again. 12–24 hr after Cmn injection, the embryos were harvested, and the brains were then subjected to the imaging analysis or electrophysiology as described below. For imaging analysis, the brains were fixed with 4% paraformaldehyde in PBS at 4°C for 2–4 hr. After equilibration with 30% (w/v) sucrose in PBS, the fixed brains were embedded in OCT compound (Sakura) and frozen. Coronal sections (10 μm thick) were prepared by cutting the frozen brains with a cryostat CM3050S (Leica), and the fluorescence of GFP and mCherry was detected using microscopies. DAPI (Sigma) was used to counterstain nuclei.

### Electrophysiology and Light Activation in Acute Slices

After *in utero* electroporation and Cmn delivery, E17.5–18.5 mice embryos were harvested, and sagittal slices (200 μm) from their neocortices were prepared in ice-cold artificial cerebral spinal fluid or ACSF (in mM: 119 NaCl, 2.5 KCl, 1.3 MgCl$_2$, 2.5 CaCl$_2$, 1 NaH$_2$PO$_4$, 26.2 NaHCO$_3$, and 11 glucose, pH 7.3) continuously bubbled with 95/5% O$_2$/CO$_2$. Vibratome slices were warmed to 33°C and incubated for 42 min in ACSF supplemented with 3 mM *myo*-inositol, 0.4 mM ascorbic acid and 2 mM sodium pyruvate, and then transferred to the recording chamber superfused with ACSF (2 ml/min).

Neurons were visualized with Hamamatsu digital camera (Model C8484) on Olympus microscope (BX51WI), and whole-cell patch-clamp recordings (Axopatch 200B) were made from neurons in the neocortex. PIRK-expressing neurons were identified by GFP and mCherry fluorescence. The internal solution contained (in mM) 130 potassium gluconate, 4 MgCl$_2$, 5 HEPES, 1.1 EGTA, 3.4 Na$_2$ATP, 10 sodium creatine phosphate, and 0.1 Na$_3$GTP at pH 7.3 with KOH. 0.5 mM BaCl$_2$ was diluted into ACSF and applied directly onto the slice. Currents were elicited with voltage ramp protocol, from −100 mV to +50 mV. For Cmn photolysis, LED with emission of 385 nm ( 190 mW; Prizmatix) was installed at the

microscope to deliver light through the objective. Light power reached the samples was measured to be 8 mW/cm$^2$. Electrophysiological chemicals were purchased from Sigma-Aldrich or Tocris Bioscience (Minneapolis, MN). Data are expressed as mean ± s.e.m. and statistical significance ($P < 0.05$) were determined by Student's t test. All measurements were made at ~33°C.

## Supplementary Material

Refer to Web version on PubMed Central for supplementary material.

## Acknowledgments

## REFERENCES

Adams SR, Tsien RY. Controlling cell chemistry with caged compounds. Annu. Rev. Physiol. 1993; 55:755–784. [PubMed: 8466191]

Beene Darren L, Dougherty Dennis A, Lester Henry A. Unnatural amino acid mutagenesis in mapping ion channel function. Curr. Opin. Neurobiol. 2003; 13:264–270. [PubMed: 12850209]

Bernstein JG, Boyden ES. Optogenetic tools for analyzing the neural circuits of behavior. Trends Cogn. Sci. 2011; 15:592–600. [PubMed: 22055387]

Bichet D, Haass FA, Jan LY. Merging functional studies with structures of inward-rectifier K(+) channels. Nat. Rev. Neurosci. 2003; 4:957–967. [PubMed: 14618155]

Bose M, Groff D, Xie J, Brustad E, Schultz PG. The incorporation of a photoisomerizable amino acid into proteins. E. coli. J. Am. Chem. Soc. 2006; 128:388–389.

Burrone J, O'Byrne M, Murthy VN. Multiple forms of synaptic plasticity triggered by selective suppression of activity in individual neurons. Nature. 2002; 420:414–418. [PubMed: 12459783]

Chow BY, Han X, Dobry AS, Qian X, Chuong AS, Li M, Henninger MA, Belfort GM, Lin Y, Monahan PE, Boyden ES. High-performance genetically targetable optical neural silencing by light-driven proton pumps. Nature. 2010; 463:98–102. [PubMed: 20054397]

Coin I, Perrin MH, Vale WW, Wang L. Photo-cross-linkers incorporated into Gprotein-coupled receptors in mammalian cells: a ligand comparison. Angew. Chem. Int. Ed. Engl. 2011; 50:8077–8081. [PubMed: 21751313]

Dart C, Leyland ML, Spencer PJ, Stanfield PR, Sutcliffe MJ. The selectivity filter of a potassium channel, murine kir2.1, investigated using scanning cysteine mutagenesis. J. Physiol. 1998; 511:25–32. [PubMed: 9679160]

England PM, Lester HA, Davidson N, Dougherty DA. Site-specific, photochemical proteolysis applied to ion channels in vivo. Proc. Natl. Acad. Sci. U. S. A. 1997; 94:11025–11030. [PubMed: 9380753]

Fehrentz T, Schonberger M, Trauner D. Optochemical genetics. Angew. Chem. Int. Ed. Engl. 2011; 50:12156–12182. [PubMed: 22109984]

Fenno L, Yizhar O, Deisseroth K. The development and application of optogenetics. Annu. Rev. Neurosci. 2011; 34:389–412. [PubMed: 21692661]

Han X. In vivo application of optogenetics for neural circuit analysis. ACS Chem. Neurosci. 2012; 3:577–584. [PubMed: 22896801]

Hibino H, Inanobe A, Furutani K, Murakami S, Findlay I, Kurachi Y. Inwardly rectifying potassium channels: their structure, function, and physiological roles. Physiol. Rev. 2010; 90:291–366. [PubMed: 20086079]

Ishii K, Yamagishi T, Taira N. Cloning and functional expression of a cardiac inward rectifier K+ channel. FEBS Lett. 1994; 338:107–111. [PubMed: 8307148]

Janovjak H, Szobota S, Wyart C, Trauner D, Isacoff EY. A light-gated, potassium-selective glutamate receptor for the optical inhibition of neuronal firing. Nat. Neurosci. 2010; 13:1027–1032. [PubMed: 20581843]

Johns DC, Marx R, Mains RE, O'Rourke B, Marban E. Inducible genetic suppression of neuronal excitability. J. Neurosci. 1999; 19:1691–1697. [PubMed: 10024355]

Kokaia M, Andersson M, Ledri M. An optogenetic approach in epilepsy. Neuropharmacology. 2013; 69:89–95. [PubMed: 22698957]

Kubo Y, Baldwin TJ, Jan YN, Jan LY. Primary structure and functional expression of a mouse inward rectifier potassium channel. Nature. 1993; 362:127–133. [PubMed: 7680768]

Kubo Y, Yoshimichi M, Heinemann SH. Probing pore topology and conformational changes of Kir2.1 potassium channels by cysteine scanning mutagenesis. FEBS Lett. 1998; 435:69–73. [PubMed: 9755861]

Lemke EA, Summerer D, Geierstanger BH, Brittain SM, Schultz PG. Control of protein phosphorylation with a genetically encoded photocaged amino acid. Nat. Chem. Biol. 2007; 3:769–772. [PubMed: 17965709]

Liu CC, Schultz PG. Adding new chemistries to the genetic code. Annu. Rev. Biochem. 2010; 79:413–444. [PubMed: 20307192]

Lu H, Klaassen C. Tissue distribution and thyroid hormone regulation of Pept1 and Pept2 mRNA in rodents. Peptides. 2006; 27:850–857. [PubMed: 16202478]

Lu T, Nguyen B, Zhang X, Yang J. Architecture of a K+ channel inner pore revealed by stoichiometric covalent modification. Neuron. 1999a; 22:571–580. [PubMed: 10197536]

Lu T, Zhu YG, Yang J. Cytoplasmic amino and carboxyl domains form a wide intracellular vestibule in an inwardly rectifying potassium channel. Proc. Natl. Acad. Sci. U. S. A. 1999b; 96:9926–9931. [PubMed: 10449796]

Matsuzaki M, Ellis-Davies GC, Nemoto T, Miyashita Y, Iino M, Kasai H. Dendritic spine geometry is critical for AMPA receptor expression in hippocampal CA1 pyramidal neurons. Nat. Neurosci. 2001; 4:1086–1092. [PubMed: 11687814]

Miller JC, Silverman SK, England PM, Dougherty DA, Lester HA. Flash decaging of tyrosine sidechains in an ion channel. Neuron. 1998; 20:619–624. [PubMed: 9581754]

Minor DL Jr, Masseling SJ, Jan YN, Jan LY. Transmembrane structure of an inwardly rectifying potassium channel. Cell. 1999; 96:879–891. [PubMed: 10102275]

Mulder J, Aguado T, Keimpema E, Barabas K, Ballester Rosado CJ, Nguyen L, Monory K, Marsicano G, Di Marzo V, Hurd YL, et al. Endocannabinoid signaling controls pyramidal cell specification and long-range axon patterning. Proc. Natl. Acad. Sci. U. S. A. 2008; 105:8760–8765. [PubMed: 18562289]

Nadeau H, McKinney S, Anderson DJ, Lester HA. ROMK1 (Kir1.1) causes apoptosis and chronic silencing of hippocampal neurons. J. Neurophysiol. 2000; 84:1062–1075. [PubMed: 10938328]

Nichols CG, Lopatin AN. Inward rectifier potassium channels. Annu. Rev. Physiol. 1997; 59:171–191. [PubMed: 9074760]

Okazaki A, Sudo Y, Takagi S. Optical silencing of C. elegans cells with arch proton pump. PLoS One. 2012; 7:e35370. [PubMed: 22629299]

Parrish AR, She X, Xiang Z, Coin I, Shen Z, Briggs SP, Dillin A, Wang L. Expanding the Genetic Code of Caenorhabditis elegans Using Bacterial Aminoacyl-tRNA Synthetase/tRNA Pairs. ACS Chem. Biol. 2012; 7:1292–1302. [PubMed: 22554080]

Philipson KD, Gallivan JP, Brandt GS, Dougherty DA, Lester HA. Incorporation of caged cysteine and caged tyrosine into a transmembrane segment of the nicotinic ACh receptor. Am. J. Physiol. Cell Physiol. 2001; 281:C195–C206. [PubMed: 11401842]

Plaster NM, Tawil R, Tristani-Firouzi M, Canun S, Bendahhou S, Tsunoda A, Donaldson MR, Iannaccone ST, Brunt E, Barohn R, et al. Mutations in Kir2.1 cause the developmental and episodic electrical phenotypes of Andersen's syndrome. Cell. 2001; 105:511–519. [PubMed: 11371347]

Priori SG, Pandit SV, Rivolta I, Berenfeld O, Ronchetti E, Dhamoon A, Napolitano C, Anumonwo J, di Barletta MR, Gudapakkam S, et al. A novel form of short QT syndrome (SQT3) is caused by a mutation in the KCNJ2 gene. Circ. Res. 2005; 96:800–807. [PubMed: 15761194]

Raimondo JV, Kay L, Ellender TJ, Akerman CJ. Optogenetic silencing strategies differ in their effects on inhibitory synaptic transmission. Nat. Neurosci. 2012; 15:1102–1104. [PubMed: 22729174]

Rhee H, Lee JS, Lee J, Joo C, Han H, Cho M. Photolytic control and infrared probing of amide I mode in the dipeptide backbone-caged with the 4,5-dimethoxy-2-nitrobenzyl group. J. Phys. Chem. B. 2008; 112:2128–2135. [PubMed: 18211054]

Saito T. In vivo electroporation in the embryonic mouse central nervous system. Nat. Protoc. 2006; 1:1552–1558. [PubMed: 17406448]

Sandoz G, Levitz J, Kramer RH, Isacoff EY. Optical control of endogenous proteins with a photoswitchable conditional subunit reveals a role for TREK1 in GABA(B) signaling. Neuron. 2012; 74:1005–1014. [PubMed: 22726831]

Sekar RB, Kizana E, Smith RR, Barth AS, Zhang Y, Marban E, Tung L. Lentiviral vector-mediated expression of GFP or Kir2.1 alters the electrophysiology of neonatal rat ventricular myocytes without inducing cytotoxicity. Am. J. Physiol. Heart Circ. Physiol. 2007; 293:H2757–H2770. [PubMed: 17675572]

Shen B, Xiang Z, Miller B, Louie G, Wang W, Noel JP, Gage FH, Wang L. Genetically encoding unnatural amino acids in neural stem cells and optically reporting voltage-sensitive domain changes in differentiated neurons. Stem Cells. 2011; 29:1231–1240. [PubMed: 21681861]

Szobota S, Isacoff EY. Optical control of neuronal activity. Annu. Rev. Biophys. 2010; 39:329–348. [PubMed: 20192766]

Tabata H, Nakajima K. Efficient in utero gene transfer system to the developing mouse brain using electroporation: visualization of neuronal migration in the developing cortex. Neuroscience. 2001; 103:865–872. [PubMed: 11301197]

Tao X, Avalos JL, Chen J, MacKinnon R. Crystal structure of the eukaryotic strong inward-rectifier K+ channel Kir2.2 at 3.1 A resolution. Science. 2009; 326:1668–1674. [PubMed: 20019282]

Wang L, Brock A, Herberich B, Schultz PG. Expanding the genetic code of Escherichia coli. Science. 2001; 292:498–500. [PubMed: 11313494]

Wang L, Schultz PG. Expanding the genetic code. Angew. Chem. Int. Ed. Engl. 2005; 44:34–66. [PubMed: 15599909]

Wang L, Xie J, Schultz PG. Expanding the genetic code. Annu. Rev. Biophys. Biomol. Struct. 2006; 35:225–249. [PubMed: 16689635]

Wang Q, Parrish AR, Wang L. Expanding the genetic code for biological studies. Chem. Biol. 2009; 16:323–336. [PubMed: 19318213]

Wang W, Takimoto JK, Louie GV, Baiga TJ, Noel JP, Lee KF, Slesinger PA, Wang L. Genetically encoding unnatural amino acids for cellular and neuronal studies. Nat. Neurosci. 2007; 10:1063–1072. [PubMed: 17603477]

Xiao J, Zhen XG, Yang J. Localization of PIP2 activation gate in inward rectifier K+ channels. Nat. Neurosci. 2003; 6:811–818. [PubMed: 12858177]

Yizhar O, Fenno LE, Davidson TJ, Mogri M, Deisseroth K. Optogenetics in neural systems. Neuron. 2011; 71:9–34. [PubMed: 21745635]

Yu CR, Power J, Barnea G, O'Donnell S, Brown HE, Osborne J, Axel R, Gogos JA. Spontaneous neural activity is required for the establishment and maintenance of the olfactory sensory map. Neuron. 2004; 42:553–566. [PubMed: 15157418]

Zaddam S, Sacconi S, Desnuelle C, Amri E, Said B. The Potassium Channel Kir2.1 Activity is Required for Osteoblastogenesis. Biophys. J. 2012; 102:538a.

Zhang F, Wang LP, Brauner M, Liewald JF, Kay K, Watzke N, Wood PG, Bamberg E, Nagel G, Gottschalk A, Deisseroth K. Multimodal fast optical interrogation of neural circuitry. Nature. 2007; 446:633–639. [PubMed: 17410168]

**A**



**B**
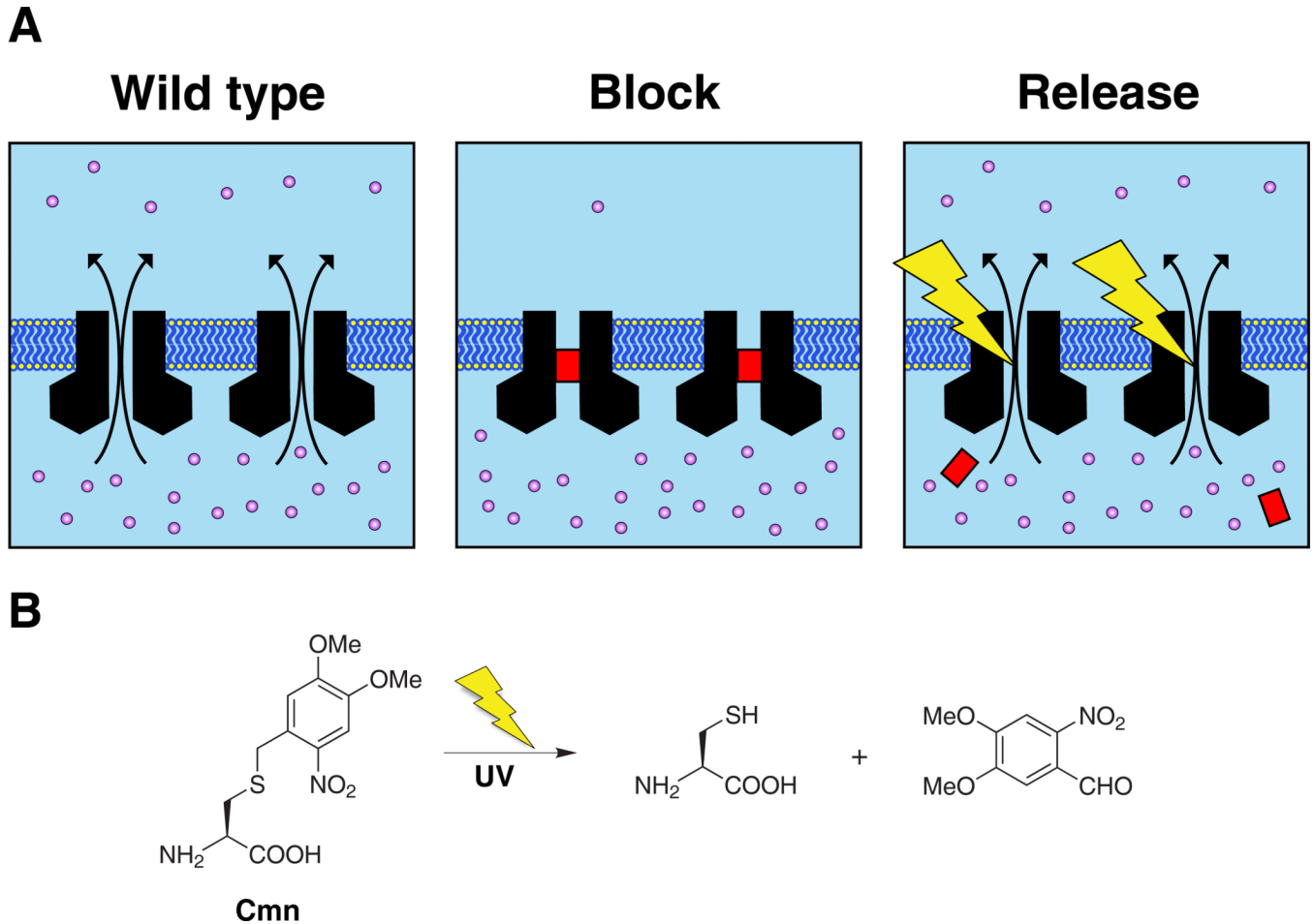


**Figure 1. Photo-activatable Inwardly Rectifying Potassium (PIRK) channel using genetic incorporation of photocaged unnatural amino acids**

(**A**) A model illustrating photo-activation of PIRK channels expressed on the plasma membrane. Left panel, wild-type Kir2.1 channels (black) conduct K+ (in purple) current in physiological conditions. Middle panel, incorporating the Uaa 4,5-dimethoxy-2-nitrobenzyl-cysteine (Cmn, in red) in the pore of Kir2.1 channels renders the channel non-conducting (PIRK channels). Right panel, UV light exposure irreversibly removes dimethoxy-nitrobenzyl group to allow permeation through the Kir2.1 channel, restoring outward K+ (in purple) current and reducing membrane excitability.

(**B**) Chemical pathway for photolysis of Cmn. UV light cleaves S – C bond, releasing dimethoxy-nitrobenzyl group from Cys. Cys would remain on the protein.
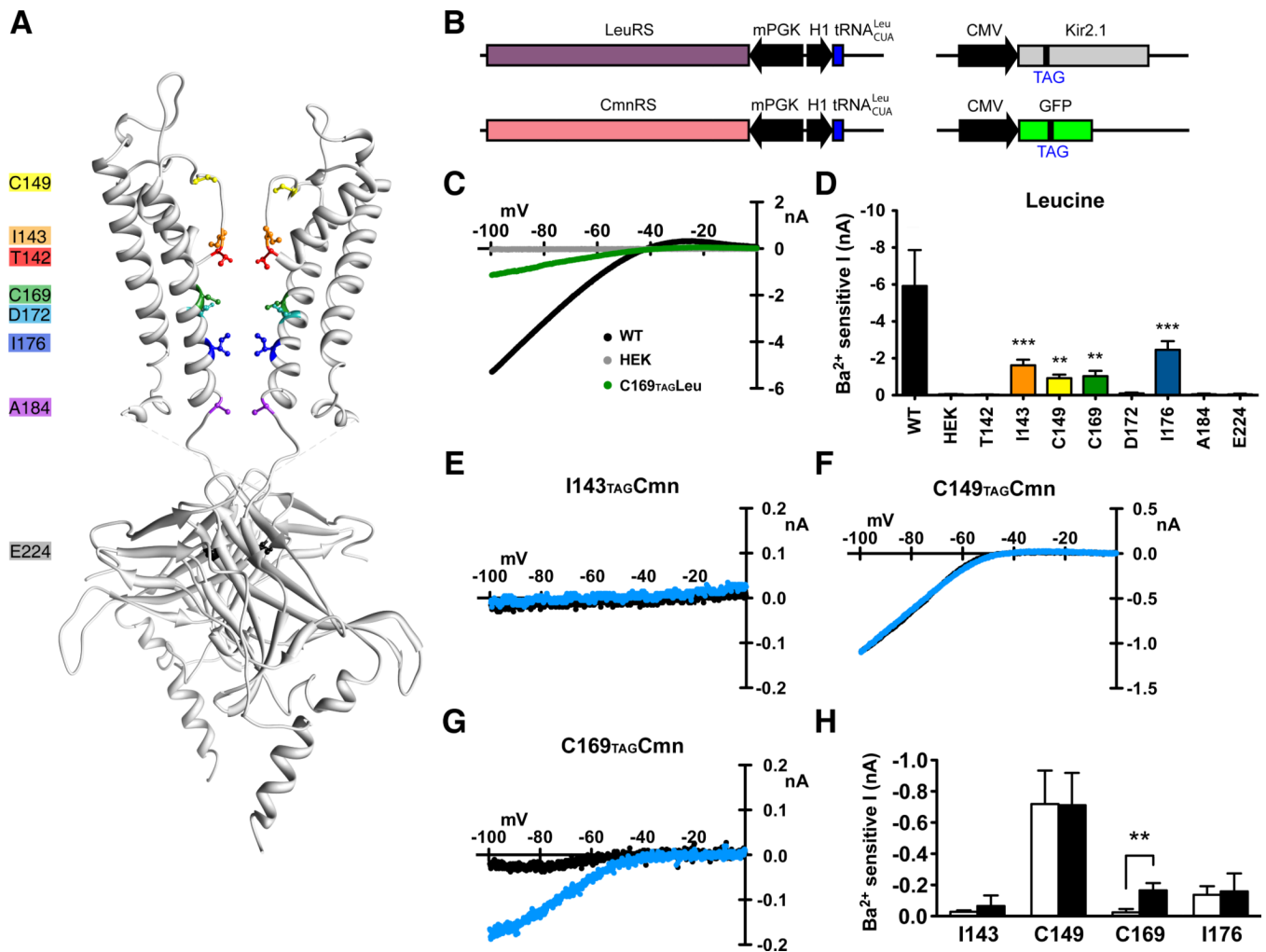
**Figure 2. Identification of a critical site in Kir2.1 for Cmn incorporation that enables photo-activation**

(**A**) Side view of the crystal structure of chicken Kir2.2 channel (PDB ID: 3JYC) showing positions of candidate sites for incorporating Cmn. Two of four subunits are shown for clarity. Eight residues that potentially contribute to ion permeation are highlighted: T142 (red), I143 (orange), C149 (yellow), C169 (green), D172 (light blue), I176 (navy), A184 (purple), and E224 (black). Molecular drawings were prepared using UCSF Chimera 1.6.2.

(**B**) Design of expression plasmids for Uaa mutagenesis. A plasmid for Leu incorporation, the amber suppressing orthogonal $tRNA_{CUA}^{Leu}$ driven by the H1 promoter and the aminoacyl-tRNA synthetase LeuRS driven by the mPGK promoter. A plasmid for Cmn incorporation, $tRNA_{CUA}^{Leu}$ driven by the H1 promoter and the aminoacyl-tRNA synthetase CmnRS driven by the mPGK promoter. A plasmid encoding Kir2.1 with the amber stop codon TAG and driven by the CMV promoter. A plasmid for the GFP reporter gene (GFP_Y182$_{TAG}$) driven by the CMV promoter.

(**C**) I–V plot of currents recorded from HEK293T cells expressing wild-type Kir2.1 ('WT'; black), expressing Kir2.1_C169$_{TAG}$Leu with $tRNA_{CUA}^{Leu}$/LueRS ('C169$_{TAG}$Leu'; green), or untransfected ('HEK'; grey).

(**D**) Mean Ba$^{2+}$ sensitive currents ($I_{Kir}$) for eight amber stop codon (TAG) mutations. Four sites in Kir2.1 were permissive for UAG suppression with Leu (I143, C149, C169 and I176).

$Ba^{2+}$-sensitive currents at $-100$ mV (mean $\pm$ s.e.m.) were: WT Kir2.1 ($-5.92 \pm 1.95$ nA, n = 4), untransfected HEK293T cells ($-0.05 \pm 0.02$ nA, n = 9), T142$_{TAG}$Leu ($-0.03 \pm 0.02$ nA, n = 5), I143$_{TAG}$Leu ($-1.62 \pm 0.30$ nA, n = 5), C149$_{TAG}$Leu ($-0.92 \pm 0.20$ nA, n = 6), C169$_{TAG}$Leu ($-1.03 \pm 0.29$ nA, n = 5), D172$_{TAG}$Leu ($-0.10 \pm 0.05$ nA, n = 5), I176$_{TAG}$Leu ($-2.46 \pm 0.47$ nA, n = 4), A184$_{TAG}$Leu ($-0.05 \pm 0.04$ nA, n = 4), and E224$_{TAG}$Leu ($-0.04 \pm 0.04$ nA, n = 4). $**P< 0.01$ and $***P< 0.001$, one-way ANOVA. WT Kir2.1 was excluded from statistical analysis.

(**E–G**) Examples of I–V plots for three different Kir2.1 channels with Cmn incorporation before (black) and after (blue) UV illumination (385 nm, 40 mW/cm$^2$, 1 sec). Cmn was incorporated at the indicated sites by the orthogonal $tRNA_{CUA}^{Leu}/CmnRS$.

(**H**) $Ba^{2+}$ sensitive current ($I_{Kir}$) measured at $-100$ mV before (open column) and after (solid column) light exposure from HEK293T cells expressing different Kir2.1 channels with Cmn incorporation. One second of 385 nm light pulse at 40 mW/cm$^2$ was applied. Only incorporation of Cmn at C169 site led to a channel where light exposure increased the current above background levels. Mean $Ba^{2+}$-sensitive currents (mean $\pm$ s.e.m.) were: I143$_{TAG}$Cmn (before: $-0.03 \pm 0.01$ nA, after: $-0.07 \pm 0.07$ nA, n = 4), C149$_{TAG}$Cmn (before: $-0.72 \pm 0.21$ nA, after: $-0.71 \pm 0.21$ nA, n = 3), C169$_{TAG}$Cmn (before: $-0.02 \pm 0.02$ nA, after: $-0.17 \pm 0.05$ nA, n = 7), and I176$_{TAG}$Cmn (before: $-0.14 \pm 0.05$ nA, after: $-0.16 \pm 0.11$ nA, n = 8). $**P< 0.01$, paired t-test.

See also Figure S1.
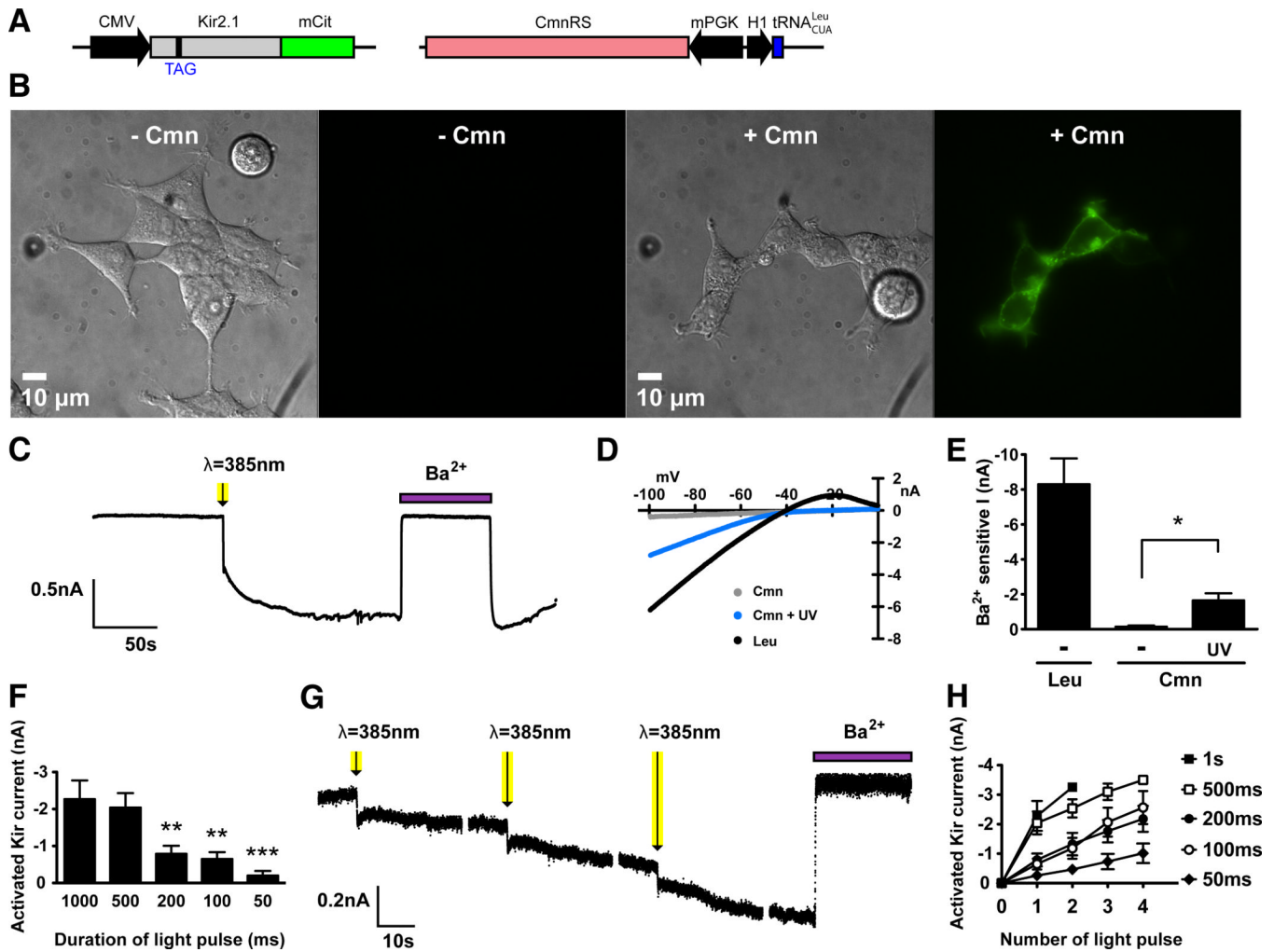
**Figure 3. Light-dependent activation of PIRK (Kir2.1_C169$_{TAG}$Cmn) expressed in HEK293T cells**

(**A**) Plasmids for PIRK expression and detection in HEK293T cells and hippocampal neurons. One plasmid encoded Kir2.1_C169$_{TAG}$ with C-terminal fusion of mCitrine (mCit) for fluorescent detection of PIRK expression, and the other plasmid encoded the tRNA$_{CUA}^{Leu}$ and CmnRS.

(**B**) Localization of PIRK channels at cell membrane. Images show PIRK-mCit expression in HEK293T cells transfected with two plasmids in (A) in the absence or presence of Cmn (1 mM) in the growth media. DIC and fluorescence images are shown. Note green fluorescence in +Cmn indicating incorporation of Cmn into Kir2.1.

(**C**) Continuous current recording at −100 mV from HEK293T cells expressing PIRK. One second pulse of light (385 nm, 40 mW/cm$^2$) activated an inward current that was inhibited by extracellular BaCl$_2$ (1 mM).

(**D**) Photo-activated PIRK currents. The I-V plot shows the currents recorded from HEK293T cells expressing Kir2.1_C169$_{TAG}$Leu (black), and PIRK before (grey) and after (blue) light activation (385 nm, 40 mW/cm$^2$, 1 sec).

(**E**) Ba$^{2+}$ sensitive current (I$_{Kir}$) measured from HEK293T cells expressing Kir2.1_C169$_{TAG}$Leu (−8.30 ± 1.48 nA, n = 7), PIRK before light activation (−0.14 ± 0.07 nA, n = 10), and PIRK after light activation (−1.65 ± 0.41 nA, n = 10). *$P$ < 0.05, paired t-test.

(**F**) PIRK activation was dependent on duration of light exposure. $Ba^{2+}$-sensitive photo-activated current was measured at −100 mV from HEK293T cells expressing PIRK after the indicated duration of light exposure (385 nm, 40 mW/cm$^2$). Mean (± s.e.m.) currents were: 1000 ms (−2.27 ± 0.51 nA, n = 5), 500 ms (−2.04 ± 0.39 nA, n = 5), 200 ms (−0.79 ± 0.22 nA, n = 8), 100 ms (−0.65 ± 0.18 nA, n = 8), and 50 ms (−0.20 ± 0.12 nA, n = 6). $**P < 0.01$ and $***P < 0.001$, one-way ANOVA.

(**G**) Stepwise activation of PIRK following multiple light pulses. Representative current trace at −100 mV shows effect of three light pulses (200 ms each, 385 nm, 40 mW/cm$^2$) applied sequentially. Extracellular $BaCl_2$ (1 mM) inhibits light-activated current confirming Kir2.1 specific current.

(**H**) Frequency dependence of light activation for PIRK channels. Mean $Ba^{2+}$-sensitive current measured at −100 mV is plotted as a function of number of light pulses (385 nm, 40 mW/cm$^2$) of different durations. 1000 ms (n = 5), 500 ms (n = 5), 200 ms (n = 8), 100 ms (n = 8), and 50 ms (n = 6). Error bars represent s.e.m..

See also Figure S2.

## Rat hippocampal primary neurons
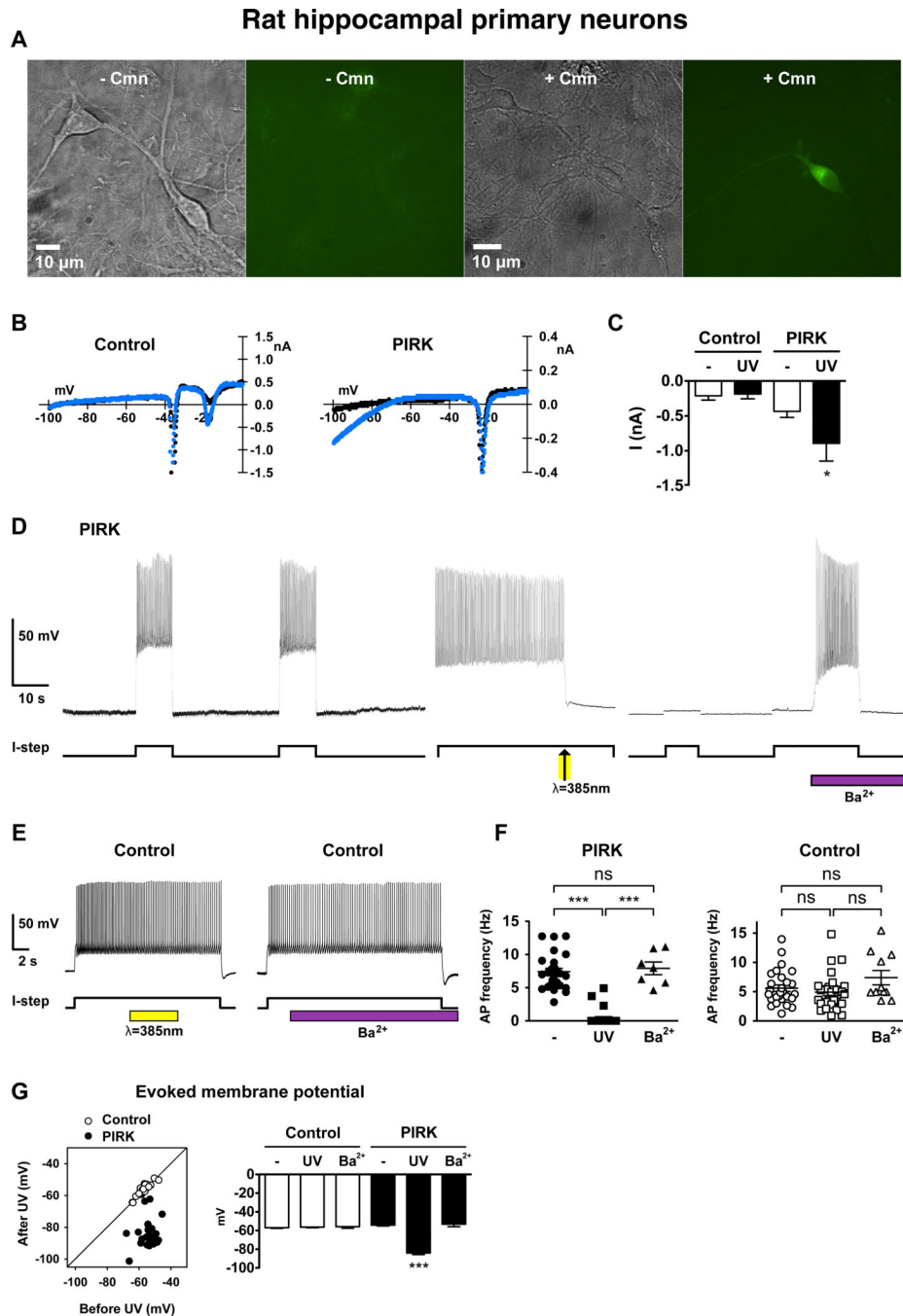


**Figure 4. Light-activation of PIRK suppresses firing of rat hippocampal neurons**
(**A**) DIC and fluorescence images of rat hippocampal neurons cultured *in vitro* and
transfected with PIRK fused to mCitrine (mCit) and $tRNA_{CUA}^{Leu}/CmnRS$ (plasmids shown in
Figure 3A) in the absence or presence of Cmn (1 mM) in the growth media. Note green
fluorescence in +Cmn indicating incorporation of Cmn.
(**B**) PIRK-expressing neurons showed photo-activated inward current. I–V plots produced
with a voltage-ramp protocol for a control neuron and a neuron expressing PIRK before
(black) and after (blue) illumination (385 nm, 40 mW/cm$^2$, 1 sec). Note inwardly rectifying
current negative to −70 mV. Rapid downward deflections likely reflect action potentials.

(**C**) Selective photo-activation of current in PIRK-expressing neurons. Currents were measured at −100 mV before (open column) and after (solid column) illumination (385 nm, 40 mW/cm$^2$, 1 sec): control neurons (before, −0.21 ± 0.06 nA; after, −0.19 ± 0.07 nA, n = 6), PIRK-expressing neurons (before, −0.43 ± 0.09 nA; after, −0.89 ± 0.25 nA, n = 6). *$P <$ 0.05, paired t-test. Currents are not leak-subtracted.

(**D**) A single light pulse suppressed firing of a hippocampal neuron expressing PIRK. Representative voltage traces recorded continuously in current-clamp. Maximal firing was evoked by 20 pA current injection ('I-step'). Light exposure (385 nm, 40 mW/cm$^2$, 1 sec, arrow) rapidly and completely suppressed neuronal firing. Firing was restored with extracellular 500 μM BaCl$_2$, which selectively inhibits Kir2.1 channels.

(**E**) Neither UV illumination alone nor BaCl$_2$ (500 μM) altered excitability of Control neurons. Maximal firing was evoked by 50 pA current injection ('I-step').

(**F**) Plot of action potential frequency of PIRK-expressing and control neurons before light, after light activation and following application of Ba$^{2+}$. One second of 385 nm light pulse at 40 mW/cm$^2$ was applied for activation. Maximal firing was elicited by a single current step (45 ± 4 pA, n = 56). Mean firing frequencies (± s.e.m.) for PIRK-expressing neurons were: before UV (7.4 ± 0.5 Hz, n = 28), after UV (0.4 ± 0.2 Hz, n = 28), and after Ba$^{2+}$ addition (7.9 ± 1.0 Hz, n = 7); values for control neurons were: before UV (5.6 ± 0.6 Hz, n = 28), after UV (4.9 ± 0.6 Hz, n = 28), after Ba$^{2+}$ addition (7.4 ± 1.2 Hz, n = 11). ***$P <$ 0.001, one-way ANOVA.

(**G**) Light activation significantly hyperpolarized PIRK-expressing neurons. One second of 385 nm light pulse at 40 mW/cm$^2$ was applied for activation. Membrane potential was measured at the evoked state (as in "**D**") after current injection. Left panel, the membrane potential after light activation is plotted as a function of membrane potential before light activation for each cell (PIRK-expression neurons: solid circle, n = 28; control neurons: open circle, n = 28). Right panel, membrane potential measured under indicated conditions was plotted. Mean (± s.e.m.) values for control neurons were: before UV (−57 ± 1 mV, n = 28), after UV (−56 ± 1 mV, n = 28), and after 500 μM BaCl$_2$ addition (−56 ± 2 mV, n = 8); for PIRK-expressing neurons: before UV (−54 ± 1 mV, n = 28), after UV (−84 ± 2 mV, n = 28), and after 500 μM BaCl$_2$ (−53 ± 3 mV, n = 7). ***$P <$ 0.001, one-way ANOVA. See also Figure S3 and S4.

**A PIRK**
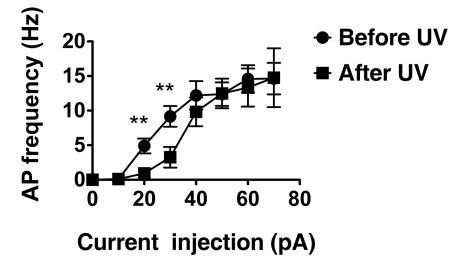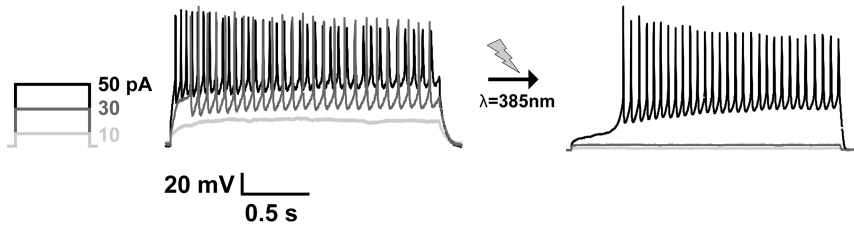
**B Control**
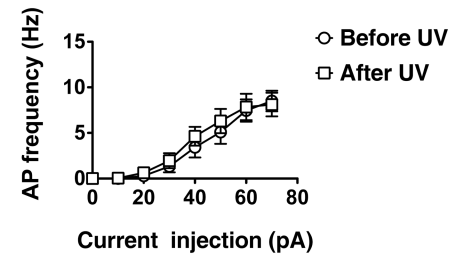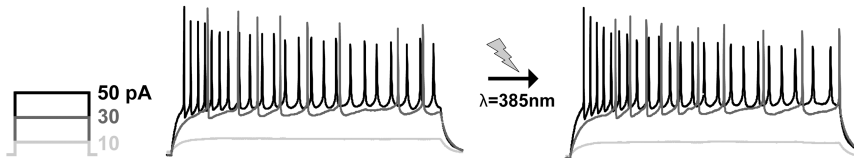
**C Rheobase**
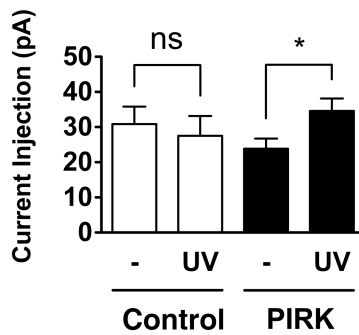
**D Resting potential**
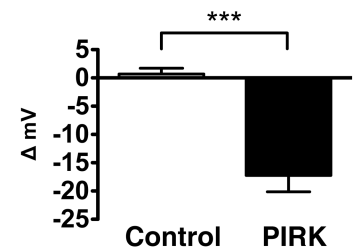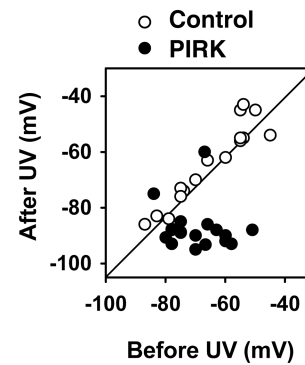
**Figure 5. Dynamic range of PIRK-dependent suppression of neuronal firing**
(**A**) In PIRK-expressing hippocampal neurons, photo-activation of PIRK significantly
decreased action potential firing frequency, dependent on current injection amplitude.
Representative voltage traces in response to three step-current injections (10 (light gray), 30
(dark gray), and 50 (black) pA) before (left) and after light exposure (385 nm, 40 mW/cm$^2$,
1 sec). Graph shows mean action potential frequency plotted as a function of current
injection amplitude (n = 13). **$P < 0.01$, paired t-test. Error bars represent s.e.m..
(**B**) In control neurons, light exposure had no effect on action potential frequency.
Representative voltage traces in response to three step-current injections (10 (light gray), 30
(dark gray), and 50 (black) pA) before (left) and after light exposure (385 nm, 40 mW/cm$^2$,
1 sec). Graph shows mean action potential frequency plotted as a function of current
injection amplitude (n = 12). Error bars represent s.e.m..
(**C**) Rheobase, the minimum current required to fire an action potential, significantly
increased in PIRK-expressing neurons upon light activation (385 nm, 40 mW/cm$^2$, 1 sec).
Mean rheobase values (mean ± s.e.m.) for control neurons were: before UV, 31 ± 5 pA; after
UV, 28 ± 6 pA, n = 12; for PIRK-expressing neurons were: before UV, 24 ± 3 pA; after UV,
35 ± 4 pA, n = 13. *$P < 0.05$, paired t-test.
(**D**) Resting membrane potential of PIRK-expressing neurons shifted to negative potentials
upon light activation (385 nm, 40 mW/cm$^2$, 1 sec). Left panel, the resting potential after

light activation is plotted as a function of the resting potential before light activation for each cell (PIRK-expressing neurons: solid circle, n = 19; control neurons: open circle, n = 19). Right panel, bar graph shows light-induced shift in resting potential. Specific values (mean ± s.e.m.) of mV were: control neurons (1 ± 1 mV, n = 19); PIRK-expressing neurons (−17 ± 3 mV, n = 19). ***$P < 0.001$, unpaired t test.

See also Figure S4.
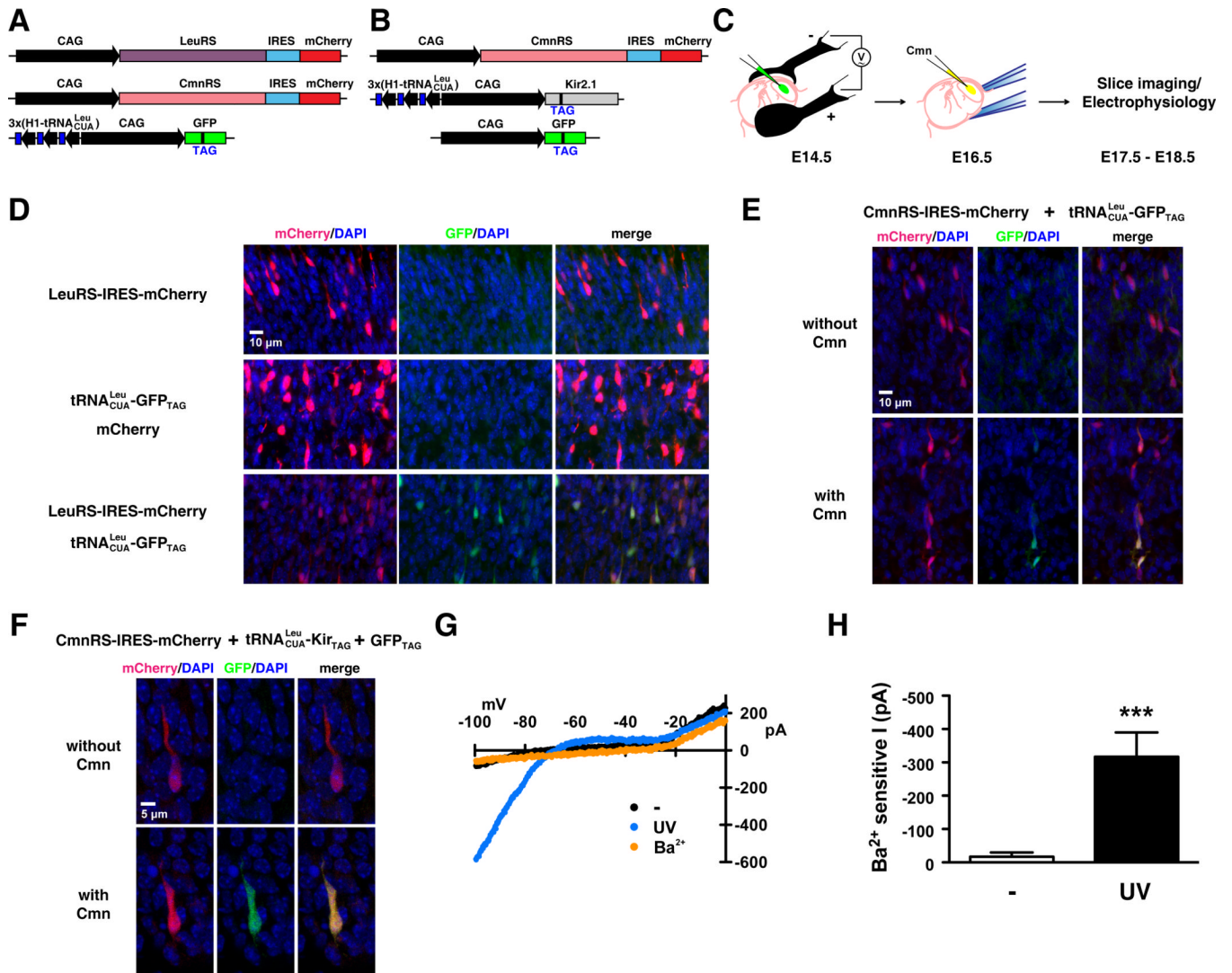
**Figure 6. *In vivo* expression of PIRK channels in the mouse neocortex**

(**A**) Validation plasmid set: one plasmid for LeuRS or for CmnRS, under the control of CAG promoter and coexpressed with mCherry via IRES sequence; one plasmid encoding

GFP_Y182$_{TAG}$ under the control of the CAG promoter. Three copies of $tRNA_{CUA}^{Leu}$ driven by the H1 promoter were combined with the GFP_Y182$_{TAG}$ to increase incorporation efficiency. Green fluorescence indicates suppression of amber codon by Leu or Cmn. Red fluorescence indicates successful gene delivery of synthetase *in vivo*.

(**B**) PIRK expression plasmid set: one plasmid for CmnRS, under the control of CAG promoter and coexpressed with mCherry via IRES sequence; one plasmid for

Kir2.1_C169$_{TAG}$ coupled with three copies of $tRNA_{CUA}^{Leu}$; one plasmid for GFP_Y182$_{TAG}$. Green and red fluorescence indicates successful expression of all three plasmids and Cmn incorporation.

(**C**) Cartoon shows experimental procedure for PIRK expression *in vivo*. Gene constructs in (**B**) were injected into the mouse neocortex (E14.5) and electroporated *in utero*. Two days later, Cmn was injected to the brain. Slice imaging and electrophysiological assay were performed on E17.5–E18.5.

(**D**) Fluorescence images of mice embryonic cortical plates showing the successful incorporation of Leu into GFP$_{TAG}$ *in vivo*. Top row: CAG-LeuRS-IRES-mCherry only. Middle row: $3 \times (\text{H1tRNA}_{\text{CUA}}^{\text{Leu}}) - \text{CAG} - \text{GFP}_{\text{TAG}}$, with CAG-mCherry as an injection marker. Bottom row: CAG-LeuRS-IRES-mCherry and $3 \times (\text{H1tRNA}_{\text{CUA}}^{\text{Leu}}) - \text{CAG} - \text{GFP}_{\text{TAG}}$. Fluorescence of mCherry and GFP was imaged in separate channels, shown with DAPI staining of DNA, and merged in the right column. GFP fluorescence was detected only when the $\text{tRNA}_{\text{CUA}}^{\text{Leu}}$, LeuRS, and GFP_Y182$_{TAG}$ were all present. Leu is present *in vivo* all the time.

(**E**) Fluorescence images of mice embryonic cortical plates showing the successful incorporation of Cmn into GFP$_{TAG}$ *in vivo*. CAG-CmnRS-IRES-mCherry and $3 \times (\text{H1tRNA}_{\text{CUA}}^{\text{Leu}}) - \text{CAG} - \text{GFP}_{\text{TAG}}$ were electroporated *in utero* in both rows. The unnatural amino acid Cmn (in the form of Cmn-Ala dipeptide) was injected *in utero* in the bottom row but not in the top row. GFP fluorescence was detected in neurons only when the $\text{tRNA}_{\text{CUA}}^{\text{Leu}}$, CmnRS, GFP_Y182$_{TAG}$, and Cmn were all present.

(**F**) Fluorescence images of mice embryonic cortical neurons showing the incorporation of Cmn into GFP$_{TAG}$ and Kir2.1$_{TAG}$ *in vivo*. The three gene constructs in (**B**) were electroporated *in utero*. GFP fluorescence was detected only with Cmn injection (bottom row), indicating Cmn incorporation in GFP$_{TAG}$ and likely Cmn incorporation in the Kir2.1$_{TAG}$.

(**G**) I–V plot of currents recorded from mice neocortical neurons showing light dependent activation of PIRK. Two days after gene constructs in (**B**) were electroporated and Cmn injected *in utero*, neocortical acute slices were prepared from embryos, as in (**C**). PIRK-expressing neurons in the slices (detected by both red and green fluorescence) were recorded before (black) and after (blue) light exposure (385 nm, 8 mW/cm$^2$, 10 sec for saturated exposure). BaCl$_2$ (500 μM) was added to verify I$_{Kir}$ after photo-activation (orange).

(**H**) Ba$^{2+}$ sensitive current (I$_{Kir}$) measured from PIRK-expressing neurons in mice neocortical slices showed significant increase upon photo-activation. I$_{Kir}$ (mean ± s.e.m.) at −100 mV was: before (−17 ± 13 pA) and after (−317 ± 73 pA) light exposure. n = 15, \*\*\**P* < 0.001, paired t-test.

See also Figure S5.